Radar Imaging Simulation for Urban Structures

Dominik Brunner, *Student Member, IEEE*, Guido Lemoine, *Member, IEEE*,
Harm Greidanus, and Lorenzo Bruzzone, *Fellow, IEEE*

***Abstract*—With the recent advent of very high resolution (VHR) spaceborne synthetic aperture radar (SAR) sensors such as TerraSAR-X and COSMO-SkyMed, the potential to use SAR simulators is increasing. In this letter, we propose a novel radar imaging simulator that is relatively simple to implement and that finds a balance between accuracy and efficiency. The main goal of the proposed method is to obtain a precise simulation of the geometry of objects in SAR images rather than a detailed radiometric simulation. The simulator is based on an extended ray-tracing procedure to determine which surfaces of a generic object contribute to the backscatter. The backscatter contributions are calculated by means of a Lambertian–specular mixture model. The simulator has already been employed successfully in a methodology for 3-D reconstruction of man-made objects from single detected VHR SAR imagery. Here, we illustrate its work on two rather different structures, a rectangular gable-roof building and an Egyptian pyramid.**

***Index Terms*—Radar imaging simulation, ray tracing, remote sensing, spaceborne synthetic aperture radar (SAR), very high resolution (VHR) images.**

I. Introduction

With the new very high resolution (VHR) synthetic aperture radar (SAR) sensors onboard the TerraSAR-X and COSMO-SkyMed satellites with spatial resolutions down to 1 m, radar imaging simulators [1] are becoming increasingly popular. They permit investigating and understanding the scattering effects of man-made targets (e.g., buildings) under a variety of configurations (e.g., different viewing angles), in a relatively easy, inexpensive, and fast manner. Furthermore, they have an important role in education, when, for instance, scene interpreters are trained to manually analyze VHR SAR imagery to extract specific information or students are familiarized with SAR and its peculiarities [2].

Various simulators with different simulation techniques and backscattering models have been proposed in literature. Scattering based on the Kirchhoff physical optics (PO) and/or geometrical optics (GO) approximations were proposed in [3] and [4], while [5] uses the finite-difference time-domain (FDTD) method, and [6] uses the integral equation method (IEM). These models take into account the roughness parameters (i.e., rms height and correlation length) and dielectric properties of the surfaces in the scene to calculate the scattering. Instead, [7] and [8] use diffuse and specular reflection, similar to the Phong shading model. For larger scenes in particular, these scattering models are often combined with ray tracing, where rays are transmitted from an antenna and traced through the scene until they return to the sensor [3], [7]. Standard ray tracing has the drawback that the rays are only reflected in the specular direction, which is a valid assumption for very smooth (metallic) surfaces. This implies that the nonspecular scattering contributions from rough surfaces are neglected. Recently, a fast simulator based on rasterization, which is supported by state-of-the-art graphical processing units, has also been presented [8].

In [9] and [10], we demonstrated how a radar imaging simulator can be employed for the 3-D reconstruction and damage assessment of man-made structures from single detected SAR imagery. The simulator is rerun many times over, searching for the best fit to the VHR SAR data. Such a scenario needs a fast simulator and aims at the extraction of information from SAR scenes over areas for which surface roughness parameters and dielectric properties are generally not known *a priori*, so that GO, PO, IEM, or FDTD cannot readily be adopted. Hence, simplified scattering models need to be used instead, which take into account the radar imaging mechanism. Rather than simulating absolute radiometric effects related to material properties and surface roughness parameters, for such models, it suffices to accurately represent the geometry of the scene and to approximate the relative differences in backscatter.

In this letter, we present in detail a new, simple to implement, yet effective radar imaging simulator (disregarding synthetic aperture effects) for urban structures that aims to precisely model the geometry of the objects in the scene and to approximate the relative radiometric differences. The proposed approach offers two novel contributions: 1) We extend standard ray tracing by adding rays reflected in multiple directions, describing also the nonspecular scattering contributions from rough surfaces, and 2) we introduce an adjustable mixture of Lambertian and specular scattering as radiometric model to calculate the backscattering from the surfaces, focusing on modeling effects related to the surface roughness while neglecting the dielectric characteristics of the materials. The simulator includes multiple-bounce scattering and can therefore simulate multiple interactions between objects, such as neighboring buildings. We demonstrate the efficiency of the proposed

Manuscript received July 8, 2009; revised October 24, 2009 and February 3, 2010; accepted February 24, 2010. Date of publication July 15, 2010; date of current version December 27, 2010.

D. Brunner is with the European Commission Joint Research Centre, 21027 Ispra, Italy, and also with the Department of Information Engineering and Computer Science, University of Trento, 38123 Trento, Italy (e-mail: dominik.brunner@jrc.ec.europa.eu).

G. Lemoine and H. Greidanus are with the European Commission Joint Research Centre, 21027 Ispra, Italy (e-mail: guido.lemoine@jrc.ec.europa.eu; harm.greidanus@jrc.ec.europa.eu).

L. Bruzzone is with the Department of Information Engineering and Computer Science, University of Trento, 38123 Trento, Italy (e-mail: lorenzo.bruzzone@disi.unitn.it).

Color versions of one or more of the figures in this paper are available online at http://ieeexplore.ieee.org.

Digital Object Identifier 10.1109/LGRS.2010.2051214

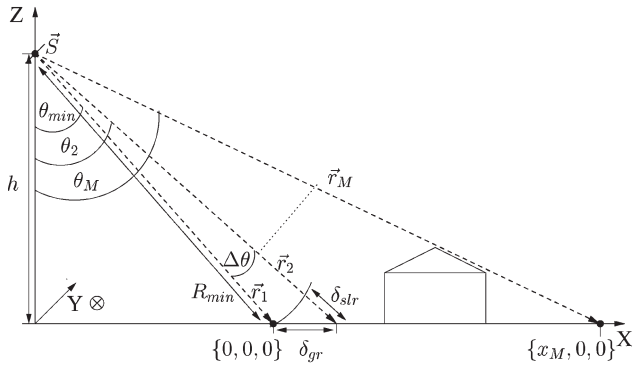

Fig. 1. Geometry of the radar imaging simulator in the range direction.

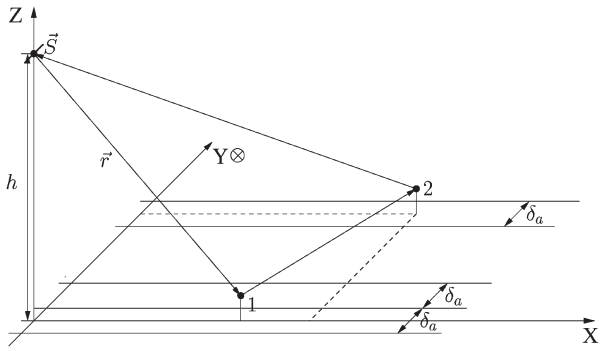

Fig. 2. Ray scattered by (1) a reflector to (2) a scatterer located outside the $\mathbf{XZ}$ plane can only return to the radar from outside the limits of the azimuth beam (which is in the $\mathbf{XZ}$ plane).

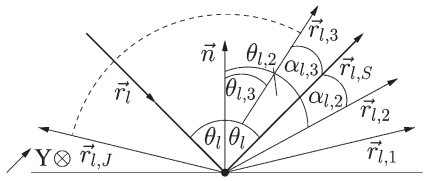

Fig. 3. Reflection of ray at the surface.

simulator in the following two examples: 1) simulation of a rectangular gable-roof building in comparison to airborne SAR data and 2) simulation of a complex-structured pyramid in comparison to TerraSAR-X spot-beam data.

II. Methodology

A. Enhanced Ray Tracing

Let us consider the geometry of the radar imaging simulator, as shown in Fig. 1, with $\theta_{\min}$ denoting the incidence angle at the near range of the scene and δ_{slr} being the slant range resolution. We fixed the scene for which the image shall be simulated (here, it is a gable-roof building) to start at the origin of a 3-D Cartesian coordinate system $\{x, y, z\} = \{0, 0, 0\}$. The scene extends horizontally in the $\mathbf{X}$- and $\mathbf{Y}$-directions and is elevated in the $\mathbf{Z}$-direction. The azimuth direction of the sensor is in the $\mathbf{Y}$-direction. h denotes the altitude of the sensor so that, considering $\theta_{\min}$, the initial sensor position is given by $\vec{S} = \{-h \cdot \tan(\theta_{\min}), 0, h\}$. The distance from the sensor to the first range bin is denoted as $R_{\min} = |\vec{S}|$. The model does not include synthetic aperture generation but, instead, directly assumes a radar beam limited in azimuth by the azimuth resolution δ_a. This contributes to the efficiency of the simulation, at the cost of disregarding specific synthetic aperture effects.

The simulator starts with the calculation of all contributions of the first azimuth resolution cell before the sensor is moved in the positive $\mathbf{Y}$-direction by δ_a to calculate the next range line. We model the radar illumination in the range direction as composition of a series of small beams with a finite cone (narrow-beam approximation), the so-called rays $r_i, i = \{1, \ldots, M\}$. The corresponding incidence angles of the individual rays $\vec{r}_i$ are denoted by θ_i. Two subsequent rays have a variation in the incidence angle by $\Delta\theta$, which is fixed by the slant range resolution at near range as

$$\Delta\theta = \left[\arccos\left(\frac{h}{R_{\min} + \delta_{\text{slr}}}\right) - \theta_{\min}\right]. \tag{1}$$

To ensure adequate sampling, $\Delta\theta$ and the azimuth step δ_a can be reduced by a factor of, e.g., two.

The number of initial rays M, which are released from the sensor per azimuth resolution cell, depends on the extent of the objects contained in the scene. It has to be high enough so that all scattering effects in the range direction (such as shadowing effects) are captured by the rays, i.e., the last range point x_M needs to be illuminated by ray $\vec{r}_M$. Hence, $M = (\theta_M - \theta_{\min})/\Delta\theta$, with $\theta_M = \arctan\{[x_M + h \cdot \tan(\theta_{\min})]/h\}$.

Each ray illuminates a small area of the surface corresponding to the resolution, giving rise to scattering in all directions. In standard ray tracing, only the specular reflected ray is considered. In our approach, we continue to trace all rays scattered within the azimuth beam plane, i.e., in the $\mathbf{XZ}$ plane. The reason for limiting to the $\mathbf{XZ}$ plane is because rays scattered out of that plane, which are bounced back to the radar, enter the radar from outside the azimuth beam and are therefore not received (see Fig. 2). The only way for a ray scattered out of the $\mathbf{XZ}$ plane to be received by the radar is if it is triple-bounced back again via a third scatterer in the $\mathbf{XZ}$ plane. These cases are therefore ignored in our model. For each traced ray, it is checked whether it scatters at another surface element. This is repeated for a definable maximum number of bounces. Tests on different models of simplified 3-D structures show that contributions from more than two bounces do not contribute significantly to the overall backscattering. All rays that travel back toward the radar contribute to the final backscatter.

The local scattering geometry is shown in Fig. 3, with $\vec{n}$ denoting the surface normal, $\vec{r}_l$ the incoming ray either coming directly from the sensor or previously reflected from a surface (multibounce contribution), θ_l the local incidence angle, $\vec{r}_{l,S}$ the ray reflected in the specular direction, $\vec{r}_{l,j}, j = \{1, \ldots, N\}$, the rays reflected in other possible directions, and $\theta_{l,j}$ the reflection angle for ray $\vec{r}_{l,j}$. The angle $\alpha_{l,j}$ is the angle between the reflected ray $\vec{r}_{l,j}$ and the specular direction $\vec{r}_{l,S}$ given by $\alpha_{l,j} = \arccos[(\vec{r}_{l,j} \cdot \vec{r}_{l,S})/(|\vec{r}_{l,j}| \cdot |\vec{r}_{l,S}|)]$, which we need in the following in order to calculate the amount of energy reflected in the direction of $\vec{r}_{l,j}$.

By limiting to rays in the $\mathbf{XZ}$ plane, we disregard the following: 1) specular reflection that could be strong but only

occurs for some peculiar geometries and 2) diffuse scattering back into the **XZ** plane that will be at a very low level.

B. Radiometric Model

The scattering of microwaves from a surface is composed by a mix of specular and Lambertian scattering, depending on the surface roughness [11]. For a perfectly smooth surface, the field is entirely scattered in the specular direction, while for a perfectly rough surface, the scattering is in all directions following the Lambertian law. The rougher is the surface, the weaker is the specular and the stronger are Lambertian components. The tracing of all rays within the **XZ** plane, explained in the previous section, enables the modeling of the Lambertian diffuse scattering component in addition to the specular reflection.

At each intersection point between a ray and a surface (bounce), the amount of energy which is returned to the sensor, as well as the amount which is scattered in the direction of a reflected ray, is calculated. The latter one determines the total amount of energy which is scattered at the next bounce (if any). The surface is modeled by elementary scattering areas of size A corresponding to the spacing of the rays and therefore of the order of the resolution. Hence, A is given by

$$A = \frac{|\vec{r}| \cdot \cos(\theta_l)}{\left[\vec{n}_x \cdot \sin(\theta_i) + \vec{n}_z \cdot \cos(\theta_i)\right]^2} \cdot \Delta\theta \cdot \delta_a \qquad (2)$$

with $\vec{n}_x$ and $\vec{n}_z$ denoting the x and z components of the surface normal, respectively. Note that the local incidence angle θ_l and the angle θ_i, which is the incidence angle for the ray directly coming from the sensor (see Fig. 1), are only the same for the first bounce contributions which occur at flat (horizontal) terrains.

The backscatter from each surface element of size A is given by $\sigma = A \cdot \sigma^\circ$, with σ° denoting the normalized radar cross section (NRCS). For the NRCS, we define the following Lambertian–specular mixture model, which is based on the bistatic Lambertian model and a specular coefficient

$$\sigma^\circ = \frac{\cos(\theta_l) \cdot \cos(\theta_{l,j}) \cdot \cos\left(\frac{\alpha_{l,j}}{2}\right)^q}{\int \cos(\theta_l) \cdot \cos(\theta_{l,j}) \cdot \cos\left(\frac{\alpha_{l,j}}{2}\right)^q d\theta_{l,j}} \cdot C \qquad (3)$$

with C being a constant determining the absolute scattering level. Since we do not intend to calculate absolute radiometry, C can be disregarded. The parameter $q \geq 0$ denotes the specularity of the surface and thus incorporates surface roughness and radar wavelength. The smoother a surface is, the larger the value of q is. In the extreme case of a perfectly smooth surface, q has to be set to infinity; to simulate a Lambertian surface, q has to be set to zero. In Fig. 4, we show the behavior of the NRCS with respect to the specularity of the surface and the reflection angles. Negative reflection angles correspond to scattering back into the quadrant of the radar, while a reflection angle of 0° shows the reflection in the direction of the surface normal, and positive reflection angles correspond to scattering forward away from the radar. The graphs show, for $q = 0$, a wide distribution with a maximum in the direction of the surface normal, whereas for smoother surfaces, the distribution becomes more peaked with a maximum in the direction of the specular reflection.

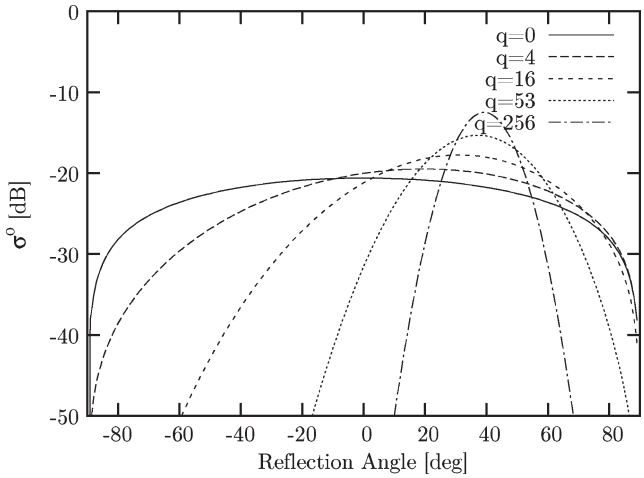

Fig. 4. NRCS using (3). The negative reflection angles correspond to backward scattering, while the positive angles are forward scattering (40° incidence angle).

Although the model implementation can accommodate coherent ray-tracing simulation, this is not used for the present application. The simulation of metallic structures, such as cars, would need a coherent approach, even allowing the exclusion of nonspecular reflection. However, since we model urban surface structures, we need to consider their roughness at X-band. In this setting, a noncoherent simulation (allowing for some specular reflection within the Lambertian–specular mixture model) is sufficient.

The 3-D object geometry is, in first instance, modeled by low-level elements, which are geometric structures with which an intersection point with the ray can be calculated. Our implementation is able to handle planes, triangles, and spheres as low-level elements. Hence, in order to simulate a building or a pyramid, the 3-D scene needs to be triangulated prior to the simulation.

III. Results

A. Gable-Roof Building

To demonstrate the results of our simulator, we choose, as first example, a midsize rectangular apartment building with a gable-roof structure, which is shown in Fig. 5(a), from Dorsten ($51°40'25''$ N, $7°00'19''$ E), Germany, which was imaged by the airborne AeS-1 sensor from Intermap Technologies GmbH. The parameters of the acquisition and the parameters used for the simulations are given in Table I. The building is made from bricks, while it is mainly surrounded by grass. Since grass has a higher surface roughness than bricks, we choose the q value for the surrounding to be smaller than that for the building. The exact values were determined empirically to produce the best resemblance with the actual data. We preprocessed the airborne data by multilooking the image by four samples in the azimuth direction and two samples in the range direction, which resulted in an equivalent number of looks of 2.59 and an approximately quadratic pixel spacing (0.64 m in azimuth

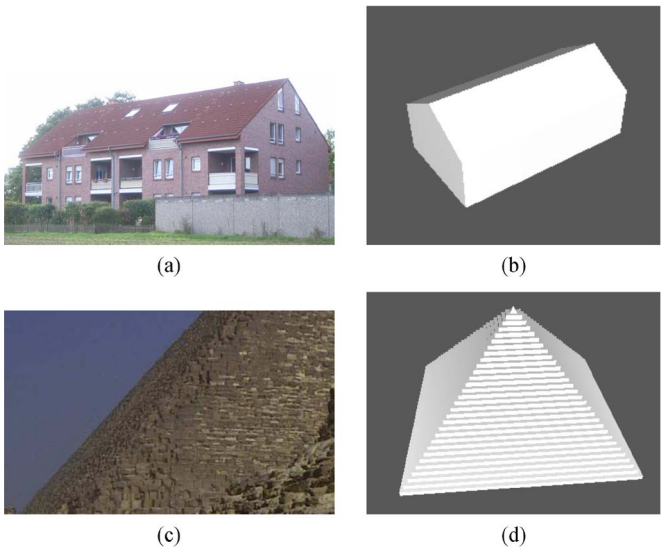

Fig. 5. (a) Photograph from the outside of the rectangular gable-roof building. (b) Three-dimensional model of the simulated building. (c) Photograph of a side of the Menkaure pyramid (photograph by Sandra Eckert). (d) Three-dimensional model of the simulated pyramid.

TABLE I
ACQUISITION PARAMETERS AND SIMULATION PARAMETERS

Parameters	Airborne / House	TerraSAR-X / Pyramid
Acquisition Date	2003-03-13	2007-07-02
Mode	-	High Resolution SpotLight
Azimuth Res.	0.16 m	1.4 m
Slant Range Res.	0.38 m	1.1 m
Incidence Angle	28° - 52°	53°
q for surrounding	12	10
q for building	20	10

and 0.76 m in slant range). The building has the dimensions 15.9 m × 27.1 m × 12.0 m (width × length × height) and a roof inclination angle of approximately 35° and was measured with 42° local incidence angle and 35° aspect angle (ground truth measured *in situ*, LIDAR digital surface model, and VHR orthophotograph).

In Fig. 6, we show the building in the actual SAR image [Fig. 6(a)] in comparison to the simulation result with speckle corresponding to 2.59 looks [Fig. 6(d)]. Fig. 5(b) shows the 3-D model, composed by 14 low-level elements, in the viewing configuration as the building was measured in the actual scene, which served as input for the simulation. Geometrically, the simulated and measured radar images coincide to within a maximum error of 1.4 m (similar for the azimuth or range direction). This discrepancy can be explained by inaccuracies in the *in situ* measurements on which the simulation is based. From the single-bounce contributions shown in Fig. 6(b), it can be concluded that the major strong scattering feature results from direct backscattering from the inclined roof. On the other hand, the L-shaped stripes in the double-bounce image [Fig. 6(c)] result from the corner reflector composed by the walls facing the sensor and the ground surface. These stripes are not apparent in the final image, because they are weak with respect to the single-bounce contributions, which is explained by the 35° aspect angle of the building [12]. The actual SAR image shows some bright spots close to the double-bounce area,

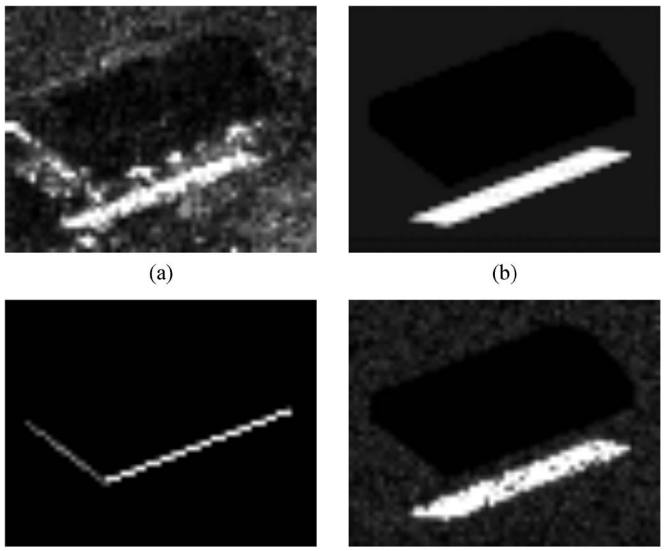

Fig. 6. Simulation result of the rectangular gable-roof building with viewing direction from the bottom. (a) Airborne SAR image (Intermap Technologies GmbH, 2003). (b) Single-bounce contribution. (c) Double-bounce contribution. (d) Final image with speckle (2.59 looks). The speckle effect is simulated using the χ^2 distribution [13]. Copyright Intermap.

which are not visible in our simulation. They can be attributed to scattering from structures at the facade, such as balconies or rain drains, which we disregarded in our simplified 3-D model. The simulation of the 82 × 69-pixel image took less than 3 s, with a memory consumption not exceeding 25 MB (Intel Core 2 Duo CPU box with 2.53-GHz 3-GB RAM and Ubuntu 9.04 32-bit operating system), highlighting the good performance of the simulator.

B. Pyramid

As a second demonstration, we compare the simulation of the Menkaure pyramid $(29°58'21''\ \text{N},\ 31°7'42''\ \text{E})$ in Giza, Egypt, to a recent TerraSAR-X image [14] (see Table I for the parameters of the acquisition and simulation). The Menkaure pyramid is 61.0 m high, with a square base of 103.4 m and an inclination angle of about 51°. The outside of the pyramid is constructed of large stone blocks that are stacked stepwise [see Fig. 5(c)]. The pyramid has a 5° aspect angle with respect to the azimuth direction of the TerraSAR-X image. Since the pyramid and its surrounding are made from materials with similar roughness, we choose the same q value for the surfaces in the scene. Note that, in [15], we used a preliminary version of this example to test a method for estimating the height for man-made structures from single detected VHR SAR imagery using an iterative simulation and feature-based matching procedure.

In Fig. 7, we show the simulation result [Fig. 7(b)] for the Menkaure pyramid in comparison to the pyramid shown in the actual SAR data [Fig. 7(a)], considering the speckle effect corresponding to 1.9 looks. Fig. 5(d) shows the 3-D model of the pyramid which is simulated (composed of 295 low-level elements) considering the viewing configuration as the pyramid was measured in the actual scene. Moreover, for this complex structure, the simulator is able to reproduce the major scattering

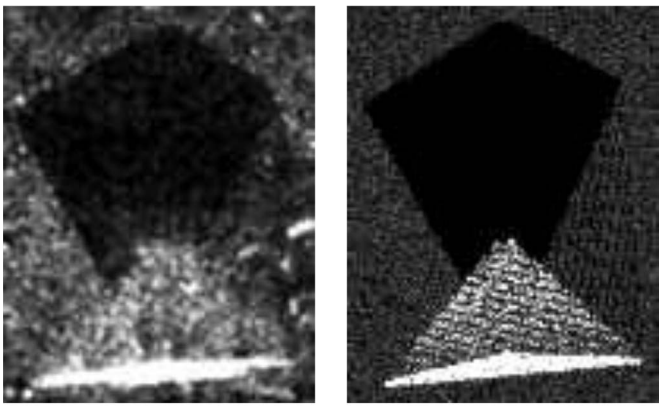

(a) (b)

Fig. 7. Simulation result of the Menkaure pyramid with viewing direction from the bottom. (a) TerraSAR-X image (DLR, 2007). (b) Final image with speckle (1.9 looks). Copyright DLR.

effects which are related to the side-looking geometry realistically. As in the previous case, the discrepancies (3 m) can be explained by inaccuracies in the *in situ* data. The simulation of the 99×126-pixel image took less than 46 s, with a memory consumption of < 116 MB.

IV. Conclusion

In this letter, we have proposed a novel, relatively simple to implement, but effective radar imaging simulator. It is based on an extended ray-tracing scheme and a Lambertian–specular mixture model, taking into account both specular and diffuse scatterings. The method aims at simulating precisely the geometry of objects in SAR rather than absolute radiometric effects related to material properties and surface roughness parameters. For the latter one, the simulator would need to be extended with a more detailed scattering model, such as the IEM, PO, GO, or FDTD, that takes into account these physical parameters. However, this would sacrifice the computational efficiency that is essential for using the model in the hypothesis–simulation–comparison loop. Moreover, due to the nature of problems analyzed with remote sensing, the values of the physical parameters are mostly not known.

To highlight the effectiveness of our approach, we showed simulation results for a gable-roof building in Dorsten, Germany, and the Menkaure pyramid in Giza, Egypt, in comparison to actual VHR SAR data. We demonstrated that the simulator based on this simplified radiometric model is sufficient to calculate effects which are related to the geometry, such as layover, shadowing, multibounce scattering, and diffuse corner reflection. The overall good resemblance between the simulations and the actual VHR SAR scenes showed that the extended ray-tracing procedure in combination with the Lambertian–specular mixture model is effective to simulate the geometry of a scene which is characterized by rough surfaces realistically. It can be noted that a pure specular model would not have produced the double-bounce component of the nonaligned object sides, which are quite strong for the pyramid example. Used in combination with techniques that compensate for the effects of an approximate radiometry, such as mutual information, this simulator is particularly suitable for advanced methodologies in information extraction scenarios, where the material properties are generally not known.

Acknowledgment

The authors would like to thank R. Günzkofer, M. Schwäbisch, and H. MacKay from Intermap Technologies GmbH, Germany, for providing the VHR airborne SAR data.

References

[1] H. Hammer, T. Balz, E. Cadario, U. Soergel, U. Thoennessen, and U. Stilla, "Comparison of SAR simulation concepts for the analysis of high resolution SAR data," in *Proc. 7th Eur. Conf. Synthetic Aperture Radar*, Friedrichshafen, Germany, Jun. 2008, pp. 213–216.

[2] T. Balz and D. Fritsch, "High-performance SAR simulation on retail video gaming consoles for education and training purposes," in *Proc. 21st ISPRS Congr.*, Beijing, China, Jul. 2008, vol. XXXVII, pp. 213–220.

[3] H.-J. Mametsa, F. Rouas, A. Berges, and J. Latger, "Imaging radar simulation in realistic environment using shooting and bouncing rays technique," in *Proc. SPIE SAR Image Anal. Model. Tech. IV*, Toulouse, France, Sep. 2001, vol. 4543, pp. 34–40.

[4] G. Franceschetti, A. Iodice, D. Riccio, and G. Ruello, "SAR raw signal simulation for urban structures," *IEEE Trans. Geosci. Remote Sens.*, vol. 41, no. 9, pp. 1986–1995, Sep. 2003.

[5] J. Delliere, H. Maître, and A. Maruani, "SAR measurement simulation on urban structures using a FDTD technique," in *Proc. Urban Remote Sens. Joint Event*, Paris, France, Apr. 2007, pp. 1–8.

[6] F. Xu and Y.-Q. Jin, "Imaging simulation of polarimetric SAR for a comprehensive terrain scene using the mapping and projection algorithm," *IEEE Trans. Geosci. Remote Sens.*, vol. 44, no. 11, pp. 3219–3234, Nov. 2006.

[7] S. Auer, S. Hinz, and R. Bamler, "Ray-tracing simulation techniques for understanding high-resolution SAR images," *IEEE Trans. Geosci. Remote Sens.*, vol. 48, no. 3, pp. 1445–1456, Mar. 2010.

[8] T. Balz and U. Stilla, "Hybrid GPU based single- and double-bounce SAR simulation," *IEEE Trans. Geosci. Remote Sens.*, vol. 47, no. 10, pp. 3519–3529, Oct. 2009.

[9] D. Brunner, G. Lemoine, L. Bruzzone, and H. Greidanus, "Building height retrieval from VHR SAR imagery based on an iterative simulation and matching technique," *IEEE Trans. Geosci. Remote Sens.*, vol. 48, no. 3, pp. 1487–1504, Mar. 2010.

[10] D. Brunner, G. Lemoine, and L. Bruzzone, "Earthquake damage assessment of buildings using VHR optical and SAR imagery," *IEEE Trans. Geosci. Remote Sens.*, vol. 48, no. 5, pp. 2403–2420, May 2010.

[11] F. T. Ulaby, R. K. Moore, and A. K. Fung, *Microwave Remote Sensing: Active and Passive*, vol. 2. Norwell, MA: Artech House, 1982.

[12] D. Brunner, L. Bruzzone, A. Ferro, and G. Lemoine, "Analysis of the reliability of the double bounce scattering mechanism for detecting buildings in VHR SAR images," in *Proc. IEEE RadarCon*, Pasadena, CA, May 2009, pp. 1–6.

[13] R. Bolter, M. Gelautz, and F. Leberl, "SAR speckle simulation," *Int. Arch. Photogramm. Remote Sens.*, vol. 21, no. B2, pp. 20–25, 1996.

[14] R. Bamler and M. Eineder, "The pyramids of Gizeh seen by TerraSAR-X—A prime example for unexpected scattering mechanisms in SAR," *IEEE Geosci. Remote Sens. Lett.*, vol. 5, no. 3, pp. 468–470, Jul. 2008.

[15] D. Brunner, G. Lemoine, and L. Bruzzone, "Height estimation of man made structures using hybrid VHR optical and SAR imagery," in *Proc. EARSeL Joint Workshop, Remote Sens.—New Challenges of High Resolution*, Bochum, Germany, Mar. 2008, pp. 186–193.